# Electronic Annex

## A spectroscopic study of solvent effects on the formation of Cu(II)-chloride complexes in aqueous solution

Ning Zhang[a,*], Jianfeng Tang[a], Yuntian Ma[b], Minghui Liang[b], Dewen Zeng[c], Glenn Hefter[d,*]

[a]*College of Science, Central South University of Forestry and Technology, Changsha 410004, Hunan, P.R. China*

[b]*CAS Center for Excellence in Nanoscience, Key Laboratory of Nanosystem and Hierarchical Fabrication, National Center for Nanoscience and Technology, Beijing 100190, P.R. China*

[c]*College of Chemistry and Chemical Engineering, Central South University, Changsha 410083, Hunan, P.R. China*

[d]*Chemistry Department, Murdoch University, Murdoch, WA 6150, Australia*

## 1. Solution composition

The composition of samples for UV-Vis and XAS measurements is collected in Table E1.

Table E1 Composition of the solutions for UV-Vis (sample nos 1 to 14) and XAS (sample nos S1 to S5) measurements.[a]

| Sample no. | $10^4$ Cu_tot (mol·kg$^{-1}$) | Cl_tot (mol·kg$^{-1}$) | $Mg(ClO_4)_2$ (mol·kg$^{-1}$) | Mg_tot (mol·kg$^{-1}$) | $Cl^-/Cu^{2+}$ ratio[b] |
|---|---|---|---|---|---|
| 1 | 4.86 | 3.38 | - | 1.69 | 6950 |
| 2 | 4.86 | 3.38 | 0.118 | 1.81 | 6950 |
| 3 | 4.86 | 3.38 | 0.277 | 1.96 | 6950 |
| 4 | 4.86 | 3.38 | 0.489 | 2.18 | 6950 |
| 5 | 4.86 | 3.38 | 0.726 | 2.41 | 6950 |
| 6 | 4.86 | 3.38 | 0.967 | 2.66 | 6950 |
| 7 | 4.86 | 3.38 | 1.14 | 2.83 | 6950 |
| 8 | 4.86 | 3.38 | 1.42 | 3.11 | 6950 |
| 9 | 4.86 | 3.38 | 1.70 | 3.39 | 6950 |
| 10 | 4.86 | 3.38 | 1.88 | 3.57 | 6950 |
| 11 | 4.86 | 3.38 | 2.19 | 3.87 | 6950 |
| 12 | 4.86 | 3.38 | 2.57 | 4.26 | 6950 |
| 13 | 4.86 | 3.38 | 2.90 | 4.58 | 6950 |
| 14 | 4.86 | 3.38 | 3.15 | 4.84 | 6950 |
| S1 | 203 | 3.26 | - | 1.63 | 161 |
| S2 | 202 | 3.25 | 0.348 | 1.97 | 161 |
| S3 | 199 | 3.22 | 0.831 | 2.44 | 162 |
| S4 | 196 | 3.19 | 1.64 | 3.23 | 163 |
| S5 | 191 | 3.14 | 2.65 | 4.22 | 164 |

[a] Concentrations and ratios contain minor round-off errors. [b] Total concentration ratio.

## 2. Molecular dynamics simulations

All MD simulations were performed using the DL_POLY_4.03 software package [1,2]; An extended simple point charge (SPC/E) model, used successfully for other brine systems [3,4], was employed for water molecules. Interactions between water molecules and the ions were defined by pairwise potentials. Long-range Coulombic interactions were handled by an Ewald summation [5] with a 12.0 Å cutoff; van der Waals interactions were modeled using the Lennard-Jones (LJ) potential. Cross terms for LJ interactions were derived from the Lorentz–Berthelot combination rules [6]. All parameters used in these calculations [7-11] are summarized in Table E2. The LJ potentials for $Cu^{2+}$, $Cl^-$ and $Mg^{2+}$ have been used previously to model the $CuCl_2$-LiCl-$H_2O$ [4] and $MgCl_2$-$H_2O$ [8] systems. The perchlorate ion, $ClO_4^-$, was assumed to be a regular rigid tetrahedron with a Cl–O distance of 1.44 Å with the parameters used previously to model the $NaClO_4$-$H_2O$ system [10].

All MD simulations used a cubic box with periodic boundary conditions and the quaternion formulation of the rotational motion equations. Prior to canonical ensemble (NVT) runs, isothermal–isobaric ensemble (NPT) runs of 4 ns were carried out to determine an appropriate volume [4,12]. Pressure was maintained at 1 atm using the Nosé–Hoover barostat [13] with a 1 ps relaxation constant. Temperature was controlled by applying the Nosé–Hoover thermostat [13]

with 1 or 0.1 ps relaxation times for NPT and NVT simulations, respectively. The Verlet velocity algorithm with a 1 fs time step was adopted, since this algorithm synchronizes the calculation of positions, velocities, and accelerations without sacrificing precision [14]. In this study, $Cu^{2+}$, $Cl^{-}$, $Mg^{2+}$, $ClO_4^{-}$ and water molecules were initially distributed randomly (Fig. E1) in a cubic box (unbiased MD simulation). Two simulations were then performed. The first (**Box-1)** was for a Cu(II), Mg(II)/$Cl^{-}$ system with 4629 particles (3 $Cu^{2+}$, 40 $Mg^{2+}$, 86 $Cl^{-}$ and 1500 $H_2O$), which corresponds approximately to a solution containing ~0.11 mol·kg$^{-1}$ $CuCl_2$ and ~1.48 mol·kg$^{-1}$ $MgCl_2$. The second (**Box-2)** was a Cu(II), Mg(II)/$Cl^{-}$, $ClO_4^{-}$ system with 5509 particles (3 $Cu^{2+}$, 120 $Mg^{2+}$, 86 $Cl^{-}$, 160 $ClO_4^{-}$ and 1500 $H_2O$) approximating a solution containing ~0.11 mol·kg$^{-1}$ $CuCl_2$, ~1.48 mol·kg$^{-1}$ $MgCl_2$ and ~2.96 mol·kg$^{-1}$ $Mg(ClO_4)_2$. These systems were calculated with total 6 ns NVT runs, including 3 ns for equilibration. The trajectory data of the last 3 ns were collected for the subsequent statistical analysis.The average residence time ($\tau_{av,j}$) of a water molecule or a chloride ion in the first and/or second hydration shells of an ion or ion cluster in both simulation boxes was calculated as

$$\tau_{av,j} = \frac{1}{N}\sum_{j=1}^{N} P_j(t, t+\Delta t)\cdot \Delta t \qquad (1)$$

where $P_j(t, t+\Delta t)$ = 0 or 1 is the probability of the species $j$ ($H_2O$ or $Cl^{-}$) being in the 1$^{st}$ solvation shell of $Cu^{2+}$ during the period $\Delta t$. The size of the solvation shell around $Cu^{2+}$ is determined by the radial distribution function (RDF) of the Cu–O pairs. The minimum cutoff radius ($R_{min}$) corresponded to the beginning point of a peak in the RDF while the maximum ($R_{max}$) corresponded to its ending point. In the defined solvation shell, there are different water molecules or $Cl^{-}$ ions frequently entering and leaving the shell. The average of their longest residence time in the shell is marked as $\tau_{av}^{max}$.

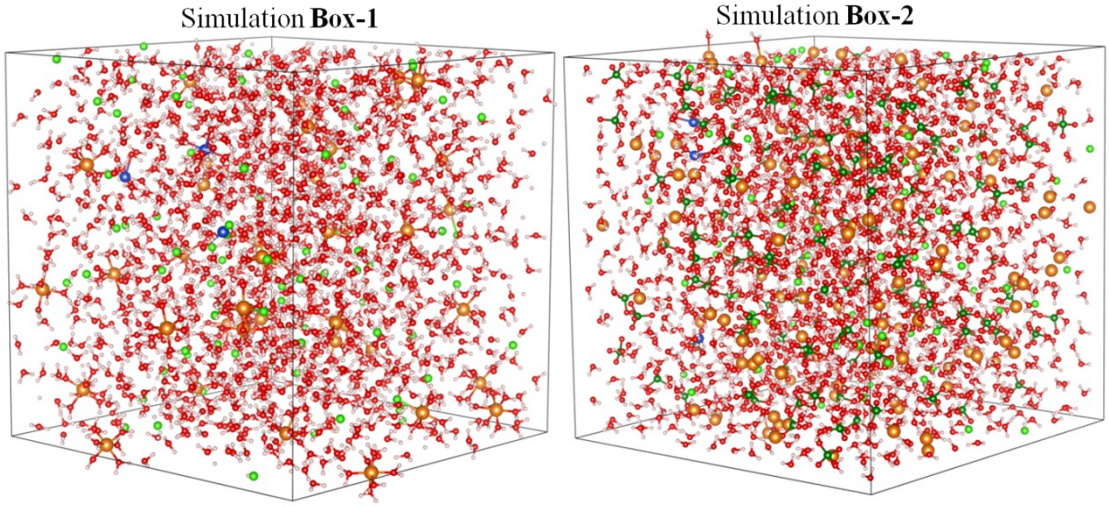


Fig. E1 Depiction of the unbiased MD simulation systems. Simulation **Box-1** with random distribution of 3 $Cu^{2+}$, 40 $Mg^{2+}$, 86 $Cl^{-}$ and 1500 $H_2O$; simulation **Box-2** with random distribution of 3 $Cu^{2+}$, 120 $Mg^{2+}$, 86 $Cl^{-}$, 160 $ClO_4^{-}$ and 1500 $H_2O$. Colors: Cu, blue; Mg, orange; free Cl, green; O, red; H, pink; Cl of $ClO_4^{-}$, dark green.

Table E2 Force field parameters for ions and water.

| Ion/water | $\varepsilon$ (kJ·mol$^{-1}$) | $\sigma$ (Å) | $q$ (e) | Ref. |
|---|---|---|---|---|
| $Cu^{2+}$ | 0.1787 | 1.8405 | 2.0000 | [5] |
| $Mg^{2+}$ | 3.663 | 1.3980 | 2.0000 | [6] |
| $Cl^{-}$ | 0.4186 | 4.4000 | –1.0000 | [7] |
| $Cl^{7+}$ | 1.109 | 3.4709 | 1.0786 | [8] |
| O | 0.8786 | 2.9599 | –0.5197 | |
| HW | 0.0000 | 0.0000 | 0.4238 | [9] |
| OW | 0.6505 | 3.1655 | –0.8476 | |

**3. Characteristic peaks of four factors**

The extracted UV-Vis characteristic peaks for four factors are collected in Table E3. As shown in Table, the peak location of each factor agrees with the previous experimental and calculated report very well. Thus, four factors 1, 2, 3 and 4 are reasonably assigned to $[CuCl]^{+}$(aq), $[CuCl_2]^{0}$(aq), $[CuCl_3]^{-}$(aq) and $[CuCl_4]^{2-}$(aq), respectively.

Table E3 Resolved UV-Vis characteristic peaks of four factors and corresponding Cu(II)-chloride complexes, along with those in previous literature for comparison.

| Components | Peak location (nm) | | | Possible species |
|---|---|---|---|---|
| | Present work | Previous experimental data [15-17] | Previous calculated data [18-20] | |
| factor 1 | ~252 | ~250 | ~250 | $[CuCl]^{+}$(aq) |
| factor 2 | ~274; ~237 | ~275; ~237 | ~270 | $[CuCl_2]^{0}$(aq) |
| factor 3 | ~234; ~278; ~385 | ~234; ~278; ~386 | ~293; ~387 | $[CuCl_3]^{-}$(aq) |
| factor 4 | ~232; ~274; ~382 | ~231; ~271; ~381 | ~287; ~382 | $[CuCl_4]^{2-}$(aq) |

**4. *q*-space EXAFS spectra**

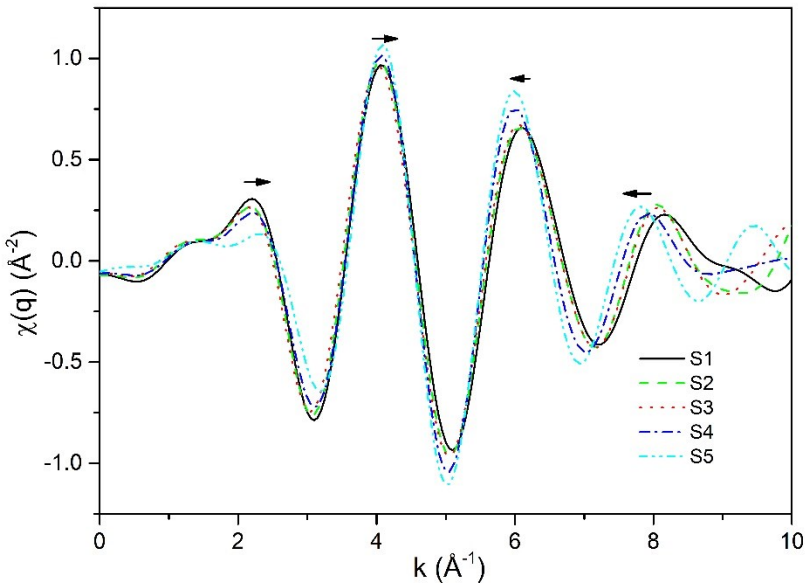


Fig. E2 Fourier transform EXAFS *q*-space spectra for **S1-S5**

**5. Fitting details for the EXAFS spectra of S3, S4 and S5**

We first used the Cu·Cl·$O_4$ unit to fit the **S3** spectrum. As the Cl ligand number is fixed to 1, using the Cu-O and Cu-Cl single scattering paths to fit its 1-3 Å R-space spectrum exhibited a bad

fitting result with the reduced $\chi_r^2$ of 804.0 and negative value of $\sigma_{Cl}^2$. This bad result mainly represents the overfitting at ~2.20 and 2.55 Å in R-space spectrum, which is ascribed to containing too many Cu-O scattering paths. Releasing the Cl ligand number, fitting result (1-3 Å R-space spectrum) shows that the structure parameters is reasonable with reduced $\chi_r^2$ of 143.7 and the Cl ligand number is 2.49 ± 0.33, indicating that there exists high-order Cu(II)-chloride complexes in **S3**. Therefore, the $Cu{\cdot}Cl_2{\cdot}O_3$ unit is used to refit the spectral data. The result shows that the fitting reduced $\chi_r^2$ drops down to 61.7, indicating that pentahedral $[CuCl_2(H_2O)_3]^0$ complexes is predominant in **S3**.

For **S4**, we first used the $Cu{\cdot}Cl_2{\cdot}O_3$ unit as the initial model to fit its spectrum. Considering the Cu-O, Cu-Cl single scattering and Cu-Cl-O-Cl double scattering paths in 1-4 Å R-space, we obtained a reasonable set of structure parameters with the reduced $\chi_r^2$ of 114.3. When releasing the Cl ligand number, the fitting gives the Cl ligand number of 2.2 with the $\chi_r^2$ of 109.6. However, by observing the fitting spectrum in 1-4 Å R-space, the deviation between the fitting and experimental spectrum is still large, especially in the range of 1-3 Å R-space. It is possible to mean that the geometry of initial guess model is unreasonable. Noted that the Cl ligand number is 2.2 (meaning the mixture of $[CuCl_2]^0$ and $[CuCl_3]^-$ complexes) if releasing the Cl ligand number in fitting and aforesaid the qualitative description of **S4** XANES spectrum exhibits the character of solution containing tetrahedral complexes. Complexes transiting from $[CuCl_2]^0$ to $[CuCl_3]^-$ is not only the change of Cl ligand number around $Cu^{2+}$ but also accompanied by the change of geometric configuration (i.e., from pentahedron to tetrahedron). Therefore, the mixed unit of pentahedral $Cu{\cdot}Cl_2{\cdot}O_3$ and tetrahedral $Cu{\cdot}Cl_3{\cdot}O$ is applied as the initial guess to refit the spectrum. We assumed that the mixed unit follows the linear relationship of [$f$ × $Cu{\cdot}Cl_2{\cdot}O_3$ + (1-$f$) × $Cu{\cdot}Cl_3{\cdot}O$]. The fitting result spectrum reproduces the experimental one very well with the fitting $\chi_r^2$ of 106.7 and $f$ of 0.64. The fitting result signifies that the pentahedral $[CuCl_2(H_2O)_3]^0$ and the tetrahedral $[CuCl_3(H_2O)]^-$ complexes are comparable in **S4**.

For **S5**, the UV-Vis data show that the $[CuCl_3]^-$ is the predominant complexes. Therefore, the tetrahedral $Cu{\cdot}Cl_3{\cdot}O$ unit is used to fit the experimental spectrum. Whether the Cl ligand number is fixed or not, all fitting results reproduce the experimental spectrum in 1-4 Å R-space very well with the $\chi_r^2$ of 75.4 and 82.8, respectively. The latter gives the Cl ligand number of 3.11, indicating that there is 89% $[CuCl_3(H_2O)]^-$ and 11% $[CuCl_4]^{2-}$ in **S5**. This is very close to the analysis of UV-Vis data. We also attempt to fit the spectrum by single tetrahedral $Cu{\cdot}Cl_4$ unit but with a bad result. The model with linear relationship of [$f$ × $Cu{\cdot}Cl_3{\cdot}O$ + (1-$f$) × $Cu{\cdot}Cl_4$] is also applied to reproduce the measured spectrum, which gives a good result with $f$ of 0.95 and $\chi_r^2$ of 83.4. These fitting results show that the tetrahedral $[CuCl_3(H_2O)]^-$ complexes is predominant but still with a spot of tetrahedral $[CuCl_4]^{2-}$ complexes in the **S5**.

**6. Analysis of $k^3$-weight spectra of S1-S5**

The fitting results of five $k^3$-weight EXAFS spectra for **S1-S5** are shown in Fig. E3. Their

structure parameters are collected in Table E4. In general, the extracted parameters in both weights (i.e., $k^2$ and $k^3$) are consistent, suggesting that the changes of UV-Vis and XAS spectra as a function of $Mg(ClO_4)_2$ concentration reflect the replacement of oxygen (water molecule) by Cl around $Cu^{2+}$.

Table E4 Cu(II) K-edge EXAFS parameters refined from the $k^3$-weight spectral data (sample nos. **S1**~**S5**) using various species and structural models.

| Sample no. | $\Delta E$(eV) | Interaction of Cu-O | | | Interaction of Cu-Cl | | | k range | R range | R-factor | $\chi_r^2$ |
|---|---|---|---|---|---|---|---|---|---|---|---|
| | | $N_O$ | $R_{Cu-O}$(Å) | $\sigma_O^2 \times 10^3$(Å$^2$) | $N_{Cl}$ | $R_{Cu-Cl}$(Å) | $\sigma_{Cl}^2 \times 10^3$(Å$^2$) | | | | |
| S1[a] | –3.38 ± 2.11 | 3.11 ± 0.39 | 1.96 ± 0.02 | 2.84 ± 1.03 | 0.85 ± 0.52 | 2.29 ±0.03 | 0.00 ± 4.52 | 2.80-10.5 | 1-4 | 0.027 | 88.4 |
| | | 1.03 ± 0.13 | 2.33 ± 0.06 | | | | | | | | |
| S2[a] | 0.75 ± 0.98 | 2.19 ± 0.23 | 1.98 ± 0.01 | 2.34 ± 0.72 | 2.08 ± 0.30 | 2.32 ±0.03 | 13.2 ± 6.01 | 2.70-11.6 | 1-4 | 0.012 | 54.6 |
| | | 0.73 ± 0.08 | 2.16 ±0.02 | | | | | | | | |
| S3[a] | –2.70 ±1.98 | 1.91 ± 0.77 | 1.97 ± 0.02 | 0.14 ± 1.93 | 2.14 ± 1.16 | 2.31 ± 0.04 | 11.2 ± 7.48 | 2.60-11.5 | 1-4 | 0.020 | 118.5 |
| | | 0.95 ± 0.39 | 2.39 ± 0.04 | | | | | | | | |
| S4[c] | 0.81 ± 1.38 | 2.0[b] (M1) | 1.91 ± 0.01 | 2.22 ± 2.06 | 2.0[b] (M1) | 2.22 ± 0.01 | 6.96 ± 1.38 | 3.00-12.05 | 1-4 | 0.027 | 66.7 |
| $f$ = 0.46 ± | | 1.0[b] (M1) | 2.21 ± 0.01 | | | | | | | | |
| 0.14 | | 1.0[b] (M2) | 2.08 ± 0.01 | | 1.0[b] (M2) | 2.16 ± 0.01 | | | | | |
| | | | | | 2.0[b] (M2) | 2.23 ± 0.01 | | | | | |
| S5[d] | –6.01 ± 2.74 | 1.0[b] (M2) | 1.92 ± 0.03 | 0.00 ± 3.64 | 1.0[b] (M2) | 2.26 ± 0.13 | 5.46 ± 4.59 | 2.9-11.0 | 1-4 | 0.022 | 57.7 |
| $f$ = 0.89 ± | | | | | 2.0[b] (M2) | 2.22 ± 0.02 | | | | | |
| 0.23 | | - | - | - | 4.0[b] (M3) | 2.39 ± 0.13 | 5.46 ± 4.59 | | | | |

[a]Sum of number of O and Cl ligands is fixed to equal to 5.
[b]Values are fixed during refinements.
[c]Model unit: $f \times$ M1 + (1-$f$) × M2; M1 = $Cu{\cdot}Cl_2{\cdot}O_3$, M2 = $Cu{\cdot}Cl_3{\cdot}O$.
[d]Model unit: $f \times$M2 + (1-$f$) × M3; M3 = $Cu{\cdot}Cl_4$.

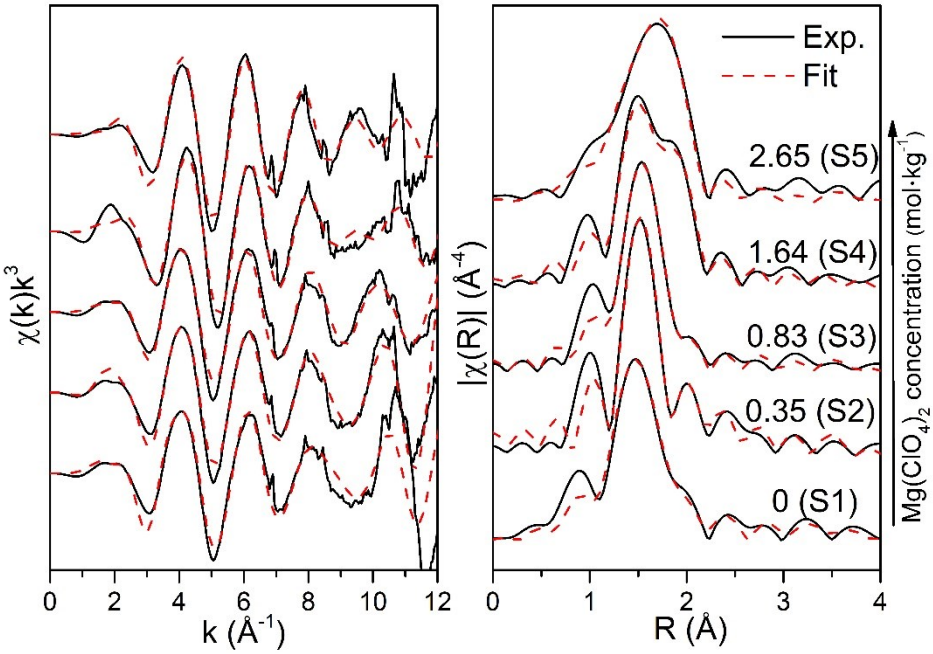


Fig. E3 Experimental (black solid lines) and fitted (red dashed lines) Cu K-edge $k^3$-weighted EXAFS spectra for the solutions containing ~0.02 mol·kg$^{-1}$ Cu(II) + ~3.2 mol·kg$^{-1}$ $Cl^-$ with various $Mg(ClO_4)_2$ concentration, shown in k- (left) and R-space (right).

**7. Molecular dynamics results**

To investigate the dynamic behavior of $H_2O$ and $Cl^-$ competitively coordinated to $Cu^{2+}$, unbiased MD simulations of **Box-1** and **Box-2** were performed. The Cu–O and Cu–Cl RDFs are plotted in Fig. E4. The first Cu–Cl peak for **Box-1** occurs at ~4.68 Å (Fig. E4a), which corresponds to $Cl^-$ in the ***outer*** (second) coordination shell of $Cu^{2+}$. No inner sphere Cu–Cl complex was apparent. This is ***inconsistent*** with the UV-Vis and XAS data presented above. However, it should be noted that similar discrepancies have been reported from MD simulations of Cu(II) in ~6 mol·kg$^{-1}$ LiCl solution [21]. Such discrepancies may indicate a need for a longer simulation time or to the use of over-simplified potential models. The models employed here predict a pseudo-octahedral coordination shell for $Cu^{2+}$ containing only strongly-bound $H_2O$ (Fig. E4c) [22]. However, experimental data [23-25] and quantum modelling [19,26], indicate that pentahedral $[Cu(H_2O)_5]^{2+}$ is the most stable aquo complex. Likewise, the **Box-2** simulation produced two $Cu^{2+}$ ions as $[Cu(H_2O)_6]^{2+}$, with the third present as $[CuCl(H_2O)_5]^+$. This resulted in average Cl/O ligand numbers around Cu of ~0.3/~5.7 (Figs.E4b and E4d).

Despite these deficiencies, it is still possible to use the present MD simulations to investigate the effects of $Mg(ClO_4)_2$ on the formation of Cu(II)/$Cl^-$ complexes. Consistent with the present UV-Vis and XAS spectra, introduction of $Mg(ClO_4)_2$ in **Box-2** caused an increase in $[CuCl(H_2O)_5]^+$. Integration of the Cl–O RDFs for both simulations (Fig. E5) showed ~7 water molecules around $Cl^-$ up to 3.7 Å, indicating addition of $Mg(ClO_4)_2$ did not significantly change the hydration of $Cl^-$.

A statistical analysis of the residence times ($\tau_{av}$ and $\tau_{av}^{max}$) of the water molecules in the ***outer***

coordination shell of $Cu^{2+}$ (from 3.5 to 4.7 Å) and around $Cl^-$ (from 2.6 to 3.8 Å) was performed for both simulations (Fig. E6). The $H_2O$ residence times (all values in ps) within these ranges is longer in simulation **Box-2** ($\tau_{av,Cu}/\tau_{av,Cl}$ = 13.0/13.8; $\tau_{av,Cu}^{max}/\tau_{av,Cl}^{max}$ = 36.6/34.5) cf. **Box-1** ($\tau_{av,Cu}/\tau_{av,Cl}$) = 12.0/11.3; $\tau_{av,Cu}^{max}/\tau_{av,Cl}^{max}$ = 24.4/19.2). These results are consistent with $Mg(ClO_4)_2$ acting as a structure maker [27,28], enhancing the H-bond network of solvent water. This interpretation is supported by the appearance of a weak peak at ~4.6 Å in the Cl-O RDF for **Box-2**, which is not observed for **Box-1**, and the slightly lower intensity of the peak at ~3.2 Å (Fig. E5).

The dynamic behavior of $Cl^-$ in the ***outer*** coordination shell of $Cu^{2+}$ (from 3.6 to 5.6 Å, Fig. E7) shows ~37 $Cl^-$ ions that frequently enter and leave this shell, with $\tau_{av} \approx 28$ ps ($\tau_{av}^{max} \approx 66$ ps) in **Box-1**, while in **Box-2** the number decreases to ~7 but with $\tau_{av} \approx 54$ ps ($\tau_{av}^{max} \approx 208$ ps). The dynamic behavior of water molecules and $Cl^-$ ions suggest that the chaotic vibrations of $Cl^-$(aq) are weakened at high ionic strengths which enhances the orientation of water molecules in the ***outer*** coordination shell of $Cu^{2+}$.

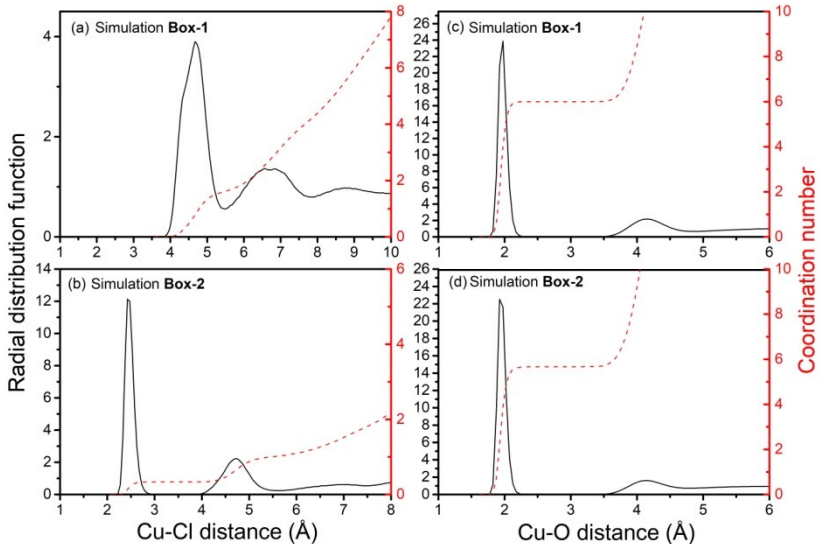


Fig. E4 Radial distribution functions for: Cu-Cl (a) and (b); and Cu-O pairs (c) and (d) of simulation **Box-1** (top) and **Box-2** (bottom) are shown with solid lines, and their integrals with dashed lines.

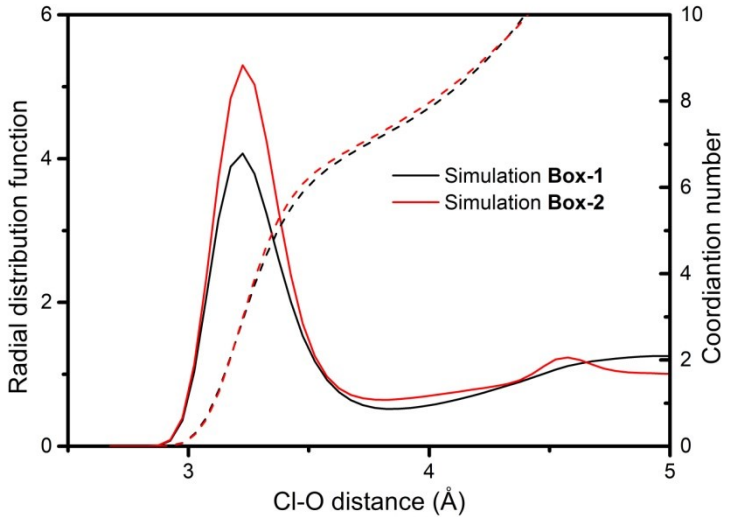


Fig. E5 Radial distribution functions for Cl-O pair of simulation **Box-1** and **Box-2** are shown with solid lines, and their integrals with dashed lines.

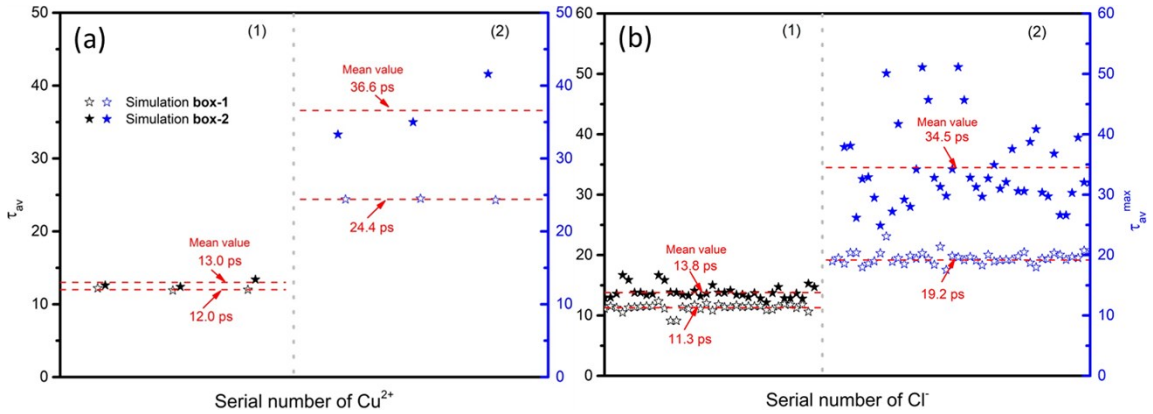


Fig. E6 Average residence time ($\tau_{av}$, (1), black) and average longest residence time ($\tau_{av}^{max}$, (2), blue) of a water molecule in the ***outer*** coordination shell of $Cu^{2+}$ (a) and in the ***inner*** hydration shell of $Cl^-$ (b) for simulations **Box-1** (hollow stars) and **Box-2** (solid stars). The red dashed lines are visual guides only, corresponding to the mean values of these times.

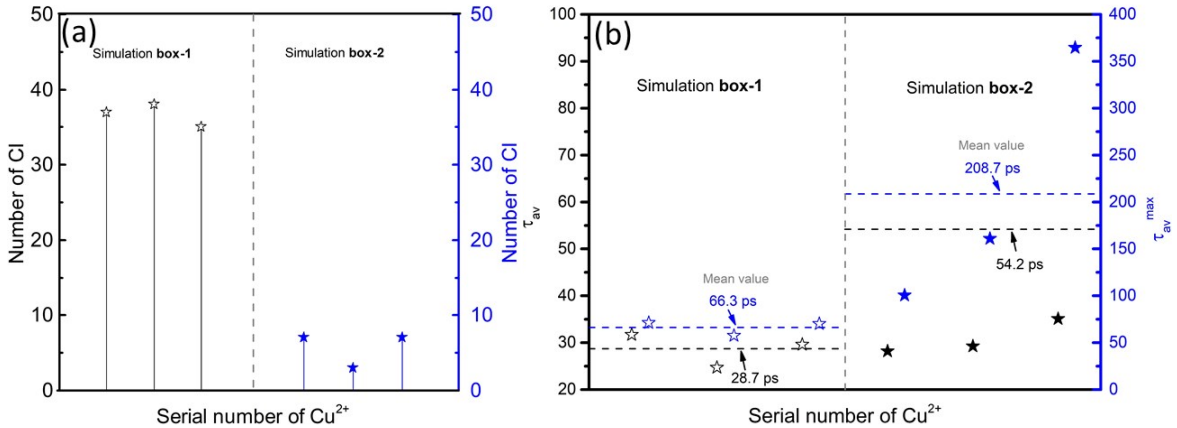


Fig. E7 Dynamic behaviors of $Cl^-$ in the outer coordination shell of $Cu^{2+}$, (a) number of $Cl^-$; (b) average residence time ($\tau_{av}$) and average longest residence time ($\tau_{av}^{max}$) of $Cl^-$ in the ***outer*** coordination shell of $Cu^{2+}$ for the simulations **Box-1** (hollow stars) and **Box-2** (solid stars). The

dashed lines are visual guides only, corresponding to the mean values of these times.

**References**


1. I.T. Todorov, W. Smith. THE DL_POLY_4 USER MANUAL Version 4.03.4. STFC Daresbury Laboratory, Daresbury, UK, 2012.
2. I.T. Todorov, W. Smith, K. Trachenko, M.T. Dove. DL_POLY_3: New dimensions in molecular dynamics simulations via massive parallelism. J. Mater. Chem. 2006, 16: 1911-1918.
3. J.L. Fulton, M. Hoffmann, J.G. Darab, B.H. Palmer. Copper(I) and copper(II) coordination structure under hydrothermal conditions at 325 °C: An X-ray absorption fine structure and molecular dynamics study. J. Phys. Chem. A 2000, 104: 11651-11663.
4. H.J. Li, H.B. Yi, J.J. Xu. High-order Cu(II) chloro-complexes in LiCl brines: Insights from density function theory and molecular dynamics. Geochim. Cosmochim. Acta 2015, 165: 1-13.
5. U. Essmann, L. Perera, M.L. Berkowitz, T. Darden, H. Lee, L.G. Pedersen. A smooth particle mesh Ewald method. J. Chem. Phys. 1995, 103: 8577-8593.
6. M.P. Allen, D.J. Tildesley. Computer Simulations of Liquids. The Ipswich Book Co Ltd, Ipswich, Suffolk, UK, 1987.
7. C.S. Babu, C. Lim. Empirical force fields for biologically active divalent metal cations in water. J. Phys. Chem. A 2006, 110: 691-699.
8. J.P. Larentzos, L.J. Criscenti. A molecular dynamics study of alkaline earth metal-chloride complexation in aqueous solution. J. Phys. Chem. B. 2008, 112: 14243-14250.
9. D.E. Smith, L.X. Dang. Computer simulations of NaCl association in polarizable water. J. Chem. Phys. 1994, 100: 3757-3766.
10. K. Nieszporek, P. Podkościelny, J. Nieszporek. Transitional hydrogen bonds in aqueous perchlorate solution. Phys. Chem. Chem. Phys. 2016, 18: 5957-5963.
11. H. Berendsen, J.R. Grigera, T.P. Straatsma. The missing term in effective pair potentials. J. Phys. Chem. 1987, 91: 6269-6271.
12. D.L. Pincus, C. Hyeon, D. Thirumalai. Effects of trimethylamine N-oxide (TMAO) and crowding agents on the stability of RNA hairpins. J. Am. Chem. Soc. 2008, 130: 7364-7372.
13. W.G. Hoover. Canonical dynamics: equilibrium phase-space distributions. Phys. Rev. A 1985, 31: 1695-1697.
14. S.A. Adcock, J.A. Mccammon. Molecular dynamics: survey of methods for simulating the activity of proteins. Chem. Rev. 2006, 106: 1589-1615.
15. J. Brugger, D.C. McPhail, J. Black, L. Spiccia. Complexation of metal ions in brines: application of electronic spectroscopy in the study of the Cu(II)-LiCl-$H_2O$ system between 25 and 90 °C. Geochim. Cosmochim. Acta 2001, 65: 2691-2708.
16. N. Zhang, Q. Zhou, X. Yin, D. Zeng. Trace amounts of aqueous copper(II) chloride complexes in hypersaline solutions: Spectrophotometric and thermodynamic studies. J. Solution Chem. 2014, 43: 326-339.
17. N. Zhang, D. Zeng, G. Hefter, Q. Chen. Chemical speciation in concentrated aqueous solutions of $CuCl_2$ using thin-film UV-visible spectroscopy combined with DFT calculations. J. Mol. Liq. 2014, 198: 200-203.
18. F. Xia, H. Yi, D. Zeng. Hydrates of copper dichloride in aqueous solution: A density functional theory and polarized continuum model investigation. J. Phys. Chem. A 2009, 113: 14029-14038.
19. F. Xia, H. Yi, D. Zeng. Hydrates of $Cu^{2+}$ and $CuCl^{+}$ in dilute aqueous solution: A density functional theory and polarized continuum model investigation. J. Phys. Chem. A 2010, 114: 8406-8416.
20. H. Yi, F. Xia, Q. Zhou, D. Zeng. $[CuCl_3]^{-}$ and $[CuCl_4]^{2-}$ hydrates in concentrated aqueous solution: A density functional theory and ab initio study. J. Phys. Chem. A 2011, 115: 4416-4426.
21. H.J. Li, H.B. Yi, J.J. Xu. High-order Cu(II) chloro-complexes in LiCl brines: Insights from density function theory and molecular dynamics. Geochim. Cosmochim. Acta 2015, 165: 1-13.
22. C.S. Babu, C. Lim. Empirical force fields for biologically active divalent metal cations in

water. J. Phys. Chem. A 2006, 110: 691-699.
23. N. Zhang, W. Wang, J. Brugger, G. Zhang, D. Zeng. Species fine structure of transition metal Cu(II) in aqueous chloride-bearing solutions: Insights from x-ray absorption spectroscopy and ab initio XANES calculations. J. Mol. Liq. 2017, 230: 200-208.
24. P. Frank, M. Benfatto, R.K. Szilagyi, P. D'Angelo, S.D. Longa, K.O. Hodgson. The solution structure of $[Cu(aq)]^{2+}$ and its implications for rack-induced bonding in blue copper protein active sites. Inorg. Chem. 2005, 44: 1922-1933
25. A. Pasquarello, I. Petri, P. Salmon, O. Parisel, T. Car, É. Tóth, D. Powell, H. Fischer, L. Helm, A. Merbach. First salvation shell of Cu(II) aqua ion: evidence for fivefold coordination. Science 2001, 291: 856-859.
26. X. Liu, X. Lu, E. Meijer, R. Wang. Hydration mechanisms of $Cu^{2+}$: tetra-, penta- or hexa-coordinated? Phys. Chem. Chem. Phys. 2010, 12: 10801-10804.
27. P. Lindqvist-Reis, A. Munoz-Paez, S. Diaz-Moreno, S. Pattanaik, I. Persson, M. Sandstrom. The structure of the hydrated gallium(III), indium(III), and chromium(III) ions in aqueous solution. A large angle x-ray scattering and EXAFS study. Inorg. Chem. 1998, 37: 6675-6683.
28. Y. Marcus. Effect of ions on the structure of water: Structure making and breaking. Chem. Rev. 2009, 109: 1346-1370.